SUPPLEMENTARY INFORMATION

Label-free detection and molecular profiling of exosomes with a nano-plasmonic sensor

Hyungsoon Im, Huilin Shao, Yong Il Park, Vanessa M. Peterson, Cesar M. Castro, Ralph Weissleder, Hakho Lee

Supplementary Methods

Soft lithography for a multi-channel flow-cell

A standard soft lithography was used for the fabrication of a multi-channel flow-cell. First, a SU-8 mold was prepared on a Si wafer through standard photolithography. A SU-8 negative resist (SU-8 2050, Microchem) was spin-coated on a Si wafer at 3500 rpm for 30 sec. The resist was then baked at 65 and 95 ˚C for 1 and 6 min, respectively. After being exposed under UV light, the resist was baked once again at 65 and 95 °C for 1 and 6 min, respectively. Then the wafer was immersed in SU-8 developed for 6 min with agitation. The developed wafer was then rinsed by isopropyl alcohol (IPA) and dried by nitrogen. The SU-8 mold was chemically treated by trichlorosilane vapor inside a desiccator for 30 min. Polydimethylsiloxane (PDMS), mixed with a curing agent with a 10:1 weight ratio and degassed, was casted on the SU-8 mold and cured on a hotplate at 60 °C for 3 hours. After curing, a PDMS block with multi-channel patterns was cut out from the mold, and inlets and outlets were cut out using 2.5 and 0.5 mm biopsy punches, respectively. After cleaning the PDMS block by acetone, IPA, and distilled water, the PDMS and nPLEX chip surfaces were treated by O_2 plasma, bonded together, and cured on a hotplate at 70 °C for 5 min.

SPR analysis

For the spectral measurements, the spectral peak position was measured using a custom-built Matlab program by fitting the transmission peak to a multi-order polynomial curve.The peak position was monitored and plotted in real-time upon a new input of data file. A minimum detection level (0.036 nm) was determined by three times of the standard deviation of the spectral peak position measured at a steady state for 5 min (See **Supplementary Fig. 7**). The limit of detection is then calculated by exploration of the minimum detection level to a fitted titration curve shown in **Fig. 2b**. For the intensity measurements, we calculated the transmitted light intensity at the nanoholes by back propagating the measured intensity profiles according to Rayleigh-Sommerfeld diffraction theory.[1] Then, a circular region-of-interest (ROI) was applied to calculate the intensity value of each sensing unit (i.e., a nanohole lattice). The transmitted light intensities were measured before and after exosome binding and the difference was normalized by the initial intensity value.

FDTD simulations

Full 3-dimensional finite-difference time-domain (FDTD) simulations were performed using a commercial software package (FDTD solutions, Lumerical). A unit cell consisted of a single nanohole with 200 nm diameter formed in a 200 nm thick Au film. Periodic boundary conditions in x- and y-directions were used to simulate an infinite array of periodic nanoholes. Nanohole arrays with different periodicities were

illuminated with a plain wave from the top (the exosome-binding side). A non-uniform mesh with a minimum grid size of 2 nm was applied. The complex dielectric constants for Au were obtained from Ref. [2] and the glass substate index was set to 1.45.

Enzyme-linked immunosorbant assay (ELISA)

Exosomes concentrated from cell culture supernatant were adsorbed onto ELISA plates (Thermo Scientific) and blocked overnight in PBS containing 1% bovine serum albumin (BSA, Sigma).[3] For titration determination, concentrated exosome stock was serially diluted in PBS before adsorption. After washing, antibodies were added in blocking solution (1 μg/mL) and incubated for 2 hours at room temperature. Following incubation with horseradish peroxidase-conjugated secondary antibody (Thermo Scientific), chemiluminescence signals were determined (Safire, Tecan).

Exosome elution and mRNA analysis

For elution experiments, we first functionalized the sensor surface with protein A/G (Thermo Scientific) and antibodies. After specific exosome capture, as determined by the real-time sensorgram (see **Supplementary Fig. 8**), we eluted bound exosomes and antibodies by incubating the sensor surface briefly with protein A/G elution buffer (Thermo Scientific) to regenerate the sensor surface and concentrate released exosomes. Eluted exosomes were immediately lysed and processed with mirVANA RNA isolation kit (Life Technologies), according to manufacturer protocol. After RNA extraction, total RNA was quantified with Nanodrop spectrophotometer (Thermo Scientific) and reverse-transcribed to generate first-strand cDNA (Applied Biosystems). Quantitative real-time polymerase chain reaction (qRT-PCR) for Taqman mRNA gene expression analyses was performed with diluted cDNA on ABI 7500 Fast Real-Time PCR system (Applied Biosystems). All procedures/experiments were performed in triplicate. Cycle threshold (Ct) values were analyzed in auto mode and manually inspected for accuracy. Relative quantification was performed for each sample by normalizing with respective GAPDH expression.[4]

Flow cytometry

Cultured adherent ovarian cells were trypsinized to form cell suspensions. Clinical ascites cells were concentrated by centrifugation and resuspended in PBS with with 0.5% BSA. All cell suspensions were labelled with antibodies (5 μg/mL) for 45 min at 4 °C. Following centrifugation and aspiration of the antibody solution, cells were labelled with FITC-conjugated secondary antibodies (Abcam) and washed twice by centrifugation. FITC fluorescence was assessed using a LSRII flow cytometer (Becton Dickinson). Mean fluorescence intensity was determined using FlowJo software, and biomarker expression levels were normalized with isotype control antibodies.

Preparation of gold nanoparticles

Spherical gold nanoparticles (Au nanospheres, diameter = 10 nm) were purchased (Nanocs), and mixed with biotin-PEG5000-thiol (4.5 mM, 100 μL; Nanocs) for biotinylation. The conjugated Au nanospheres was collected via filtration (Amicon Ultra, Millipore). The star-shaped gold nanoparticles (Au nanostars) were synthesized using seed-mediated growth method.[5] First, seed Au nanoparticles were prepared through citrate reduction of $HAuCl_4$, as previously reported.[6] The size of the seed particles was 12 nm. The seed particles (200 μL) were then added to $HAuCl_4$ (0.25 mM, 10 mL) containing HCl (1 M, 10 μL). To the mixture, $AgNO_3$ (2 mM, 100 μL) and ascorbic acid (0.1 M, 50 μL) were sequentially added to initiate the

particle growth. The reaction was completed in 30 sec. The prepared Au nanostars were mixed with biotin-PEG5000-thiol (4.5 mM, 100 μL; Nanocs), and processed for biotinylation as mentioned above.

nPLEX signal amplification using gold nanoparticles

Exosomes captured on the nPLEX sensor were subjected to secondary gold nanoparticle labeling for signal enhancement. Briefly, captured exosomes were exposed to biotinylated anti-CD63 antibody (Ancell, 10 μg/mL). After washing, neutravidin (Thermo Scientific, 10 μg/mL) was introduced as a linker into the fluidic channel, before subsequent injection of biotinylated gold nanoparticles. For control channels, equivalent amount of biotinylated IgG istyope control antibody (Ancell) was used to target the captured exosomes.

Statistical analysis

For the clustering analyses, all protein profiling markers were first sorted and categorized into four different groups (cancer only, ubiquitous, benign only, absent), according to their expression status in cancer and benign cell lines (defined by whether the markers were present or absent in either benign or malignant cells). Subsequently, the markers in each category were clustered using ($1 - P$) as the distance metric (P, Pearson correlation). Receiver operation characteristic (ROC) curves for CD63, EpCAM and CD24 were generated from patient profiling data. Note that we used exosomal expression (ξ) of EpCAM and CD24. When combining EpCAM and CD24 profiles, we used an arithmetic average of EpCAM and CD24 levels as an independent variable. The optimal cutoff value for each marker was established by determining the point closest to the top-left corner (perfect sensitivity or specificity) of the ROC curve. All diagnostic metrics (i.e., sensitivity, specificity, accuracy) were calculated using standard formulas. The empirical ROC curves were smoothed with the binormal fitting model. We used the R package (version 3.0.2) for ROC curve analyses.

Western blotting analysis

Exosomes concentrated via ultracentrifugation were lysed in radio-immunoprecipitation assay buffer containing protease inhibitors (Thermo Scientific) and quantified using the bicinchoninic acid assay (BCA assay, Thermo Scientific). Protein lysates were resolved by sodium dodecyl sulfate polyacrylamide gel electrophoresis (SDS-PAGE) and transferred onto polyvinylidene fluoride membrane (PVDF, Invitrogen) and immunoblotted with antibodies against exosomal markers: HSP90 (Cell Signaling), HSP70 (BD Biosciences), Flotillin 1 (BD Biosciences), Flotillin 2 (BD Biosciences), CD9 (Santa Cruz) and CD63 (Santa Cruz); and other vesicular markers: Integrin β1 (Cell Signaling) and Integrin α5 (Cell Signaling). Following incubation with horseradish peroxidase-conjugated secondary antibody (Cell Signaling), enhanced chemiluminescence was used for immunodetection (Thermo Scientific).

Scanning electron microscopy

All samples were fixed with half-strength Karnovsky's fixative and washed twice with PBS. After dehydration in a series of increasing ethanol concentrations, samples were transferred for critical drying (Samdri, Tousimis) and subsequently coated with platinum/palladium using a sputter coater (208HR, Cressington Scientific Instruments), before imaging with a scanning electron microscope (Supra55VP, Carl Zeiss).

Transmission electron microscopy

Exosomes were fixed with 2% paraformaldehyde and transferred onto EM grid. Adsorbed vesicles were washed and subjected to contrast staining with uranyl oxalate (4%) and methyl cellulose (2%) mixture. After air dry, the sample was imaged with a transmission electron microscope (JOEL 2100)

Supplementary Figures

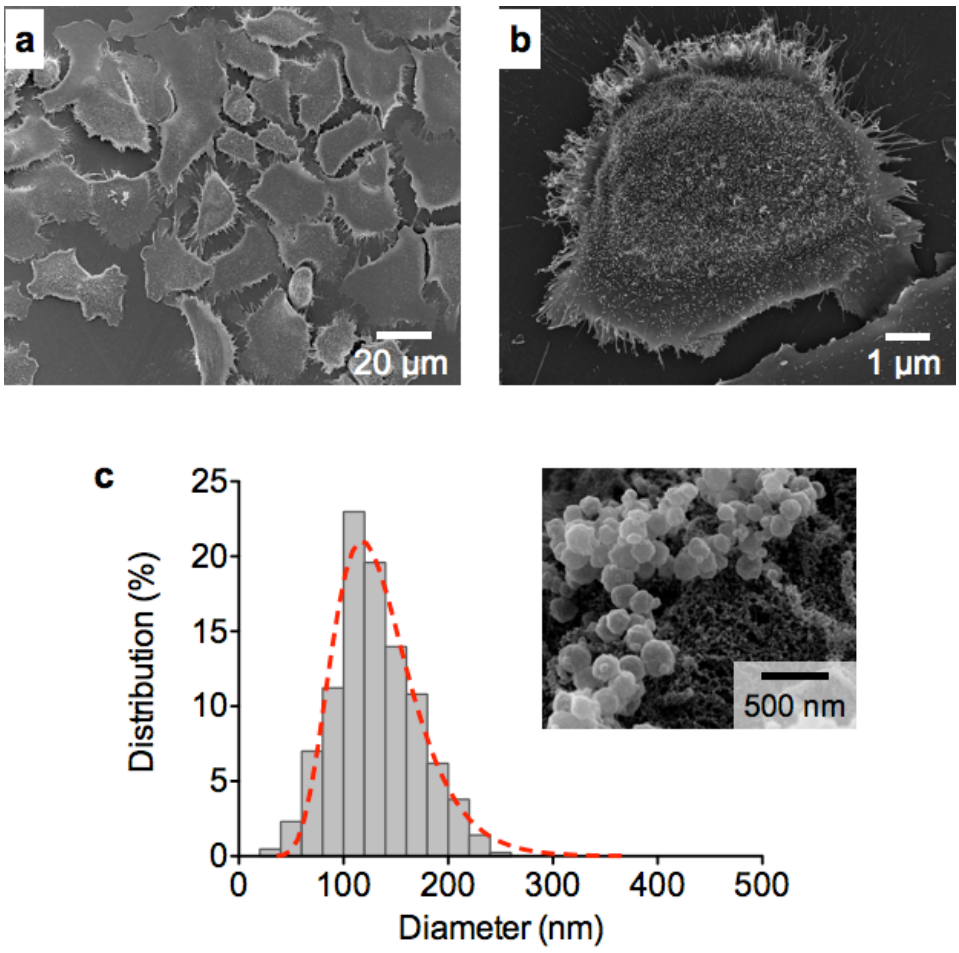

Supplementary Figure 1. Exosomes shed by cancer cells. (a, b) CaOV3 ovarian cancer cells shed nanoscale vesicles as imaged by a scanning electron microscope (SEM). **(c)** The size distribution of exosomes, characterized by the nanoparticle tracking analysis. The mean diameter of exosomes was ~ 100 nm, which agreed with the SEM observation (inset).

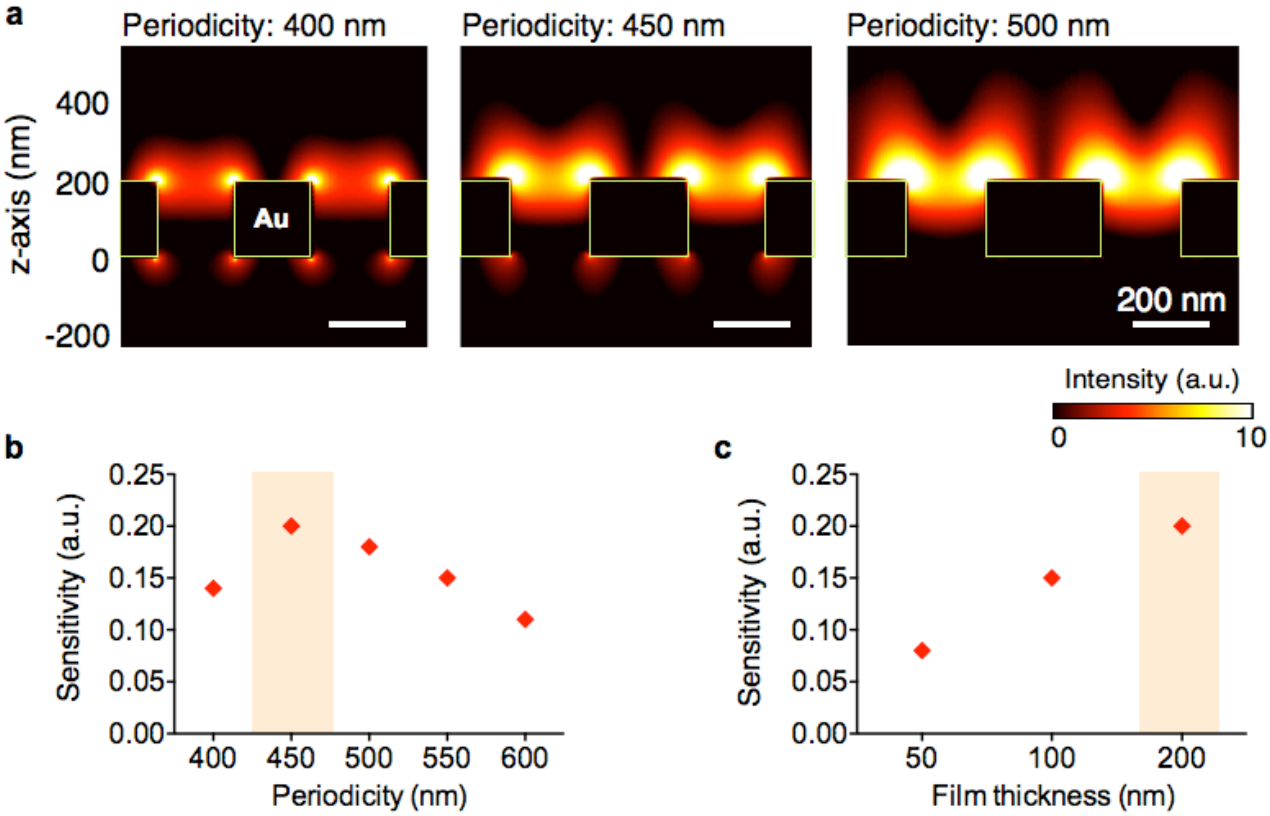

d

Hole diameter (nm)	Thickness (nm)	Periodicity (nm)	Spectral shift (nm)	Peak width (nm)	Sensitivity
200	50	450	3.3	40	0.08
200	100	450	4.3	29	0.15
200	200	400	3.7	27	0.14
200	200	450	4.1	21	0.20
200	200	500	3.8	21	0.18
200	200	550	3.2	21	0.15
200	200	600	2.2	20	0.11

Supplementary Figure 2. Sensitivity optimization of the nPLEX system. (a) The electric field intensity of the nPLEX sensor is simulated. The decay length of the intensity increases with longer periodicity. **(b)** Simulated detection sensitivity of the sensor for 100 nm exosomes, defined as $\Delta\lambda/w$, has the maximal value with the 450-nm nPLEX sensor. **(c)** For 200 nm hole diameter and 450 nm periodicity, the sensitivity maximized at 200 nm Au film thickness. **(d)** Summary of simulation data for nanohole design. The optimal dimension for the highest sensitivity is highlighted. a.u., arbitrary unit.

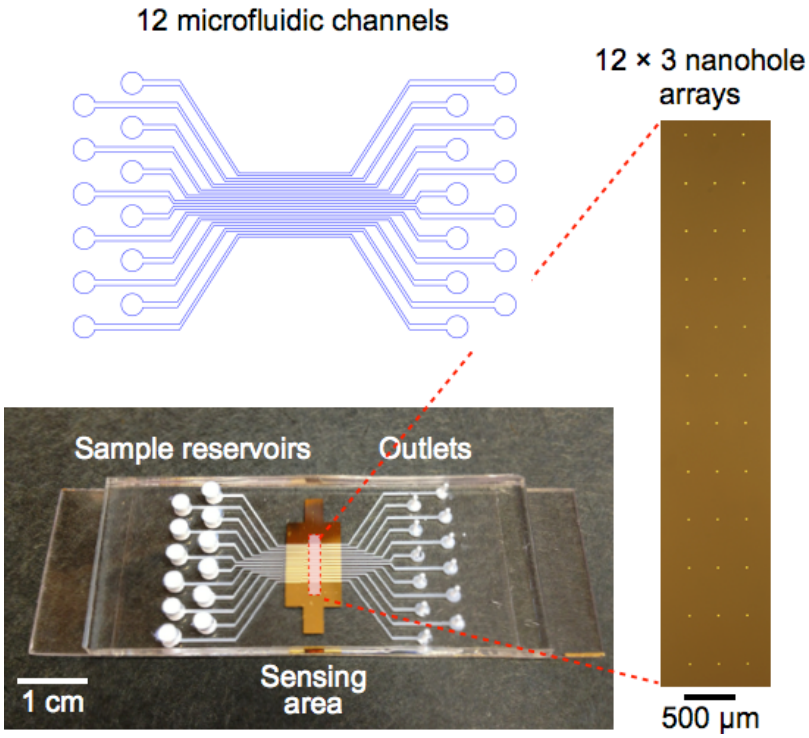

Supplementary Figure 3. Device configuration. A 12-channel fluidic cell (top) was placed on top of a glass slide containing nanohole arrays (bottom). A total of 36 measurement sites were arranged into a 12 × 3 array format (right) with each fluidic channel encompassing three measurement sites. Surface functionalization, sample injection, and washing steps were performed through the multi-channel microfluidic system.

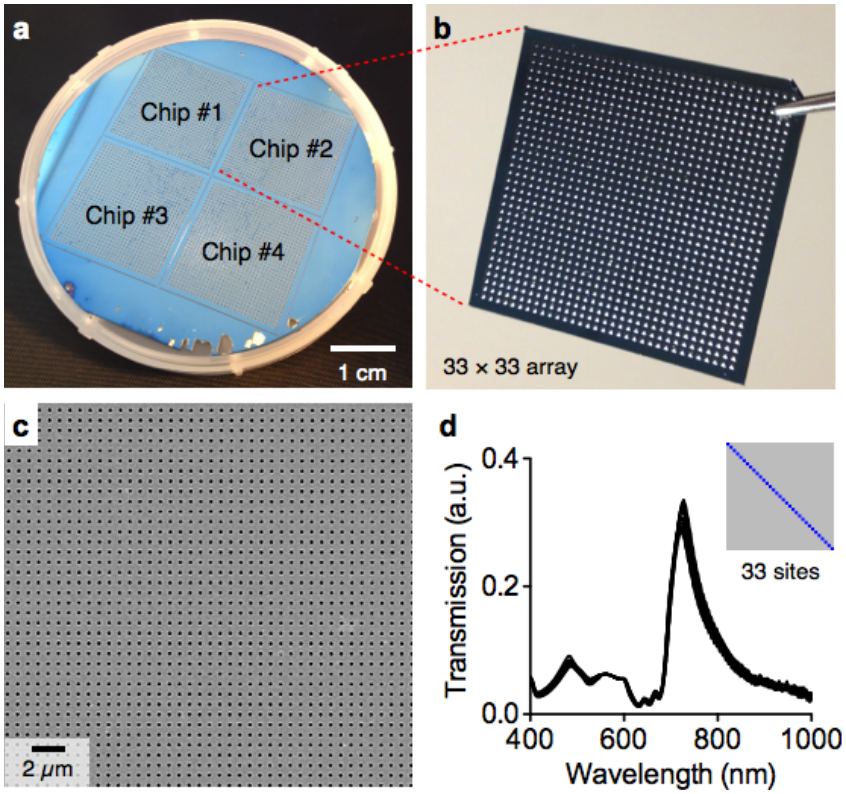

Supplementary Figure 4. Second generation nPLEX chip. (a) By applying light interference lithography[7,8], we patterned the entire 4-inch wafer with nanoholes. The sensing area was defined by anisotropic backside etching of the Si wafer. **(b)** The nPLEX chip has 1,089 (33 × 33) measurement sites for massively parallel detection. **(c)** Magnified views of the nanohole lattice. Each measurement site has a 200 × 200 nanohole lattice. The hole diameter is 200 nm, and the periodicity is 450 nm. **(d)** Transmission spectra, measured from 33 diagonal sites (inset), closely matched one another. This result confirmed that highly uniform nanohole arrays were patterned across the wafer. a.u., arbitrary unit.

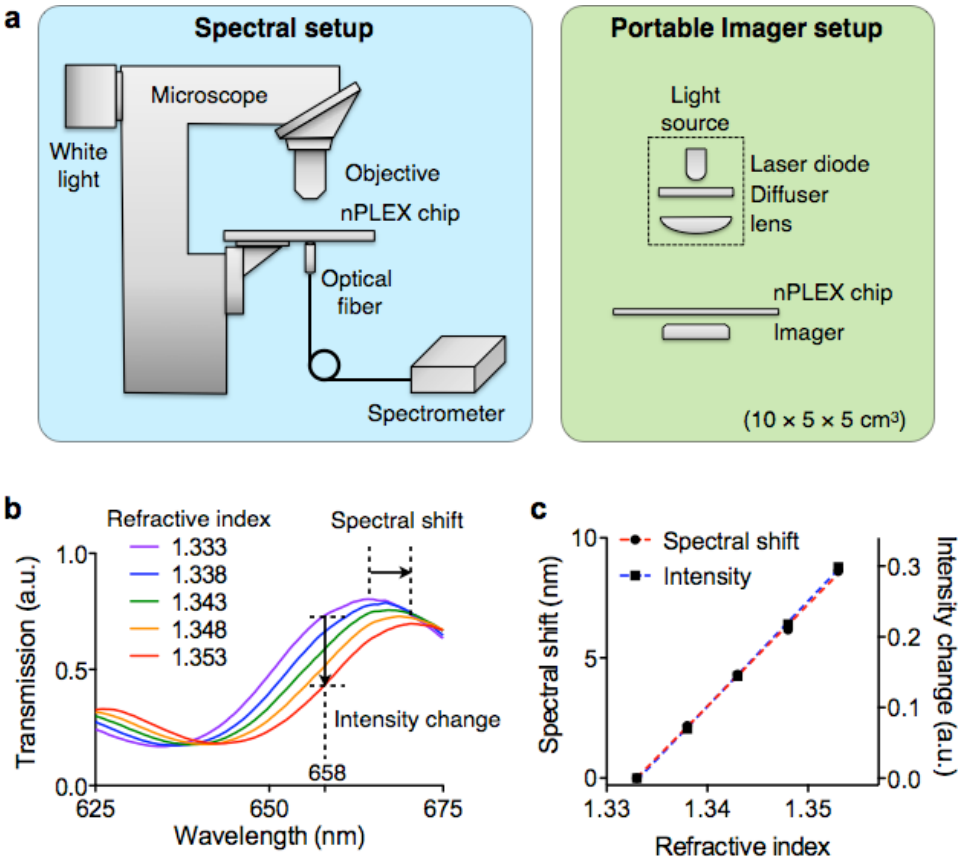

Supplementary Figure 5. nPLEX measurement setups. (a) (Left) A spectrometer setup was constructed on a conventional upright microscope. A tungsten white light source illuminated the nPLEX sensor through a 10× microscope objective, and the transmitted light was collected by an optical fiber placed underneath the nPLEX sensor. The collected light was then analyzed by a miniaturized spectrometer. **(Right)** The portable imaging setup consisted of a light source (a laser diode) and a CMOS imager. The nPLEX sensor was located on top of the imager and the transmitted light intensities through the nanohole arrays were recorded by the imager. **(b)** Exosome binding increases the refractive index on the sensor surface, which induces a spectral shift to a longer wavelength. This increase of refractive index also causes intensity changes at a fixed laser wavelength. Exosome binding, therefore, can be detected either by tracking spectral shifts in the spectrometry setup or by measuring the intensity changes in the portable imaging setup. **(c)** Both spectral shifts and intensity changes showed linear responses to the refractive index. a.u., arbitrary unit.

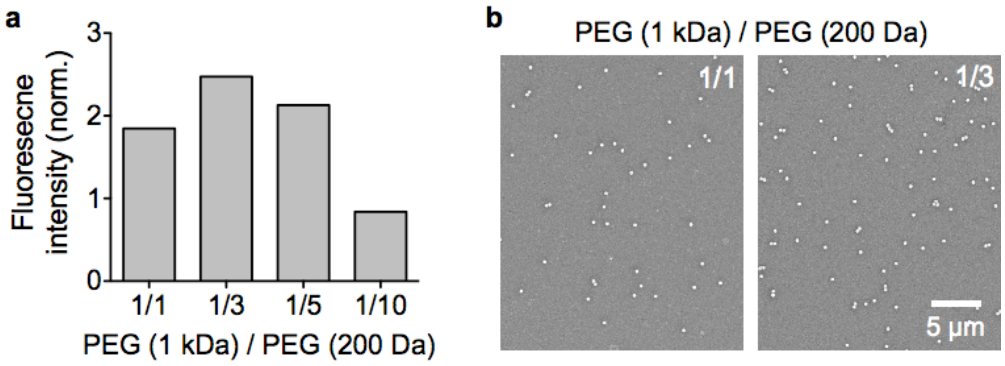

Supplementary Figure 6. Optimization of surface chemistry. (a) Biotinylated, fluorescent polystyrene beads (diameter, 100 nm) were captured on streptavidin-coated sensor surface. These sensors were functionalized with mixtures of long (MW, 1 kDa) and short (MW, 200 Da) polyethylene glycol (PEG) polymers. Streptavidin was conjugated on long PEGs. Following the bead capture, the fluorescence intensity of a streptavidin-coated sensor was normalized against that of a control sensor (without streptavidin functionalization). The 1:3 mixture of long and short PEGs showed the best capture yield. **(b)** Electron micrographs of sensor surfaces PEGylated with 1/1 and 1/3 mixture of long and short PEGs. More beads were captured when the ratio was 1/3, supporting the fluorescent data in (a).

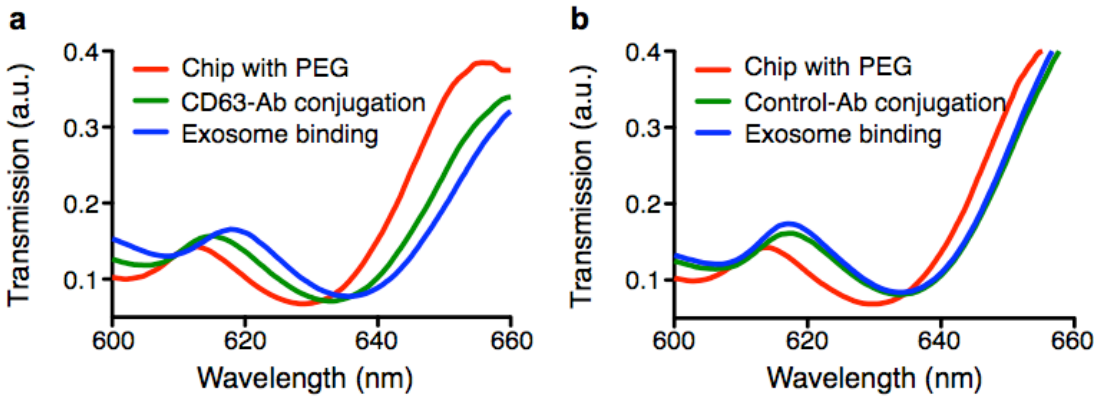

c

Antibody	Net spectral shift (nm)	
	After antibody conjugation	After Exosome capture
CD63	3.71 ± 0.35	2.49 ± 0.01
IgG control	3.76 ± 0.29	0.10 ± 0.00

Supplementary Figure 7. Spectral shifts upon antibody (Ab) conjugation and specific exosome binding. (a, b) nPLEX chips were conjugated with either CD63 (a) or IgG control (b) antibodies. Exosomes from human ovarian cancer cells (CaOV3) were subsequently introduced. Transmission spectral shifts associated with antibody conjugation and specific exosome binding were measured. Similar spectral shifts were observed for both CD63 and control antibody conjugation, which indicated similar extent of antibody grafting onto the sensor surface. Exosome binding, however, was only observed with the CD63-specific chip (a); the control chip (b) displayed negligible binding. **(c)** Summary of spectral shifts in both sensors. a.u., arbitrary unit.

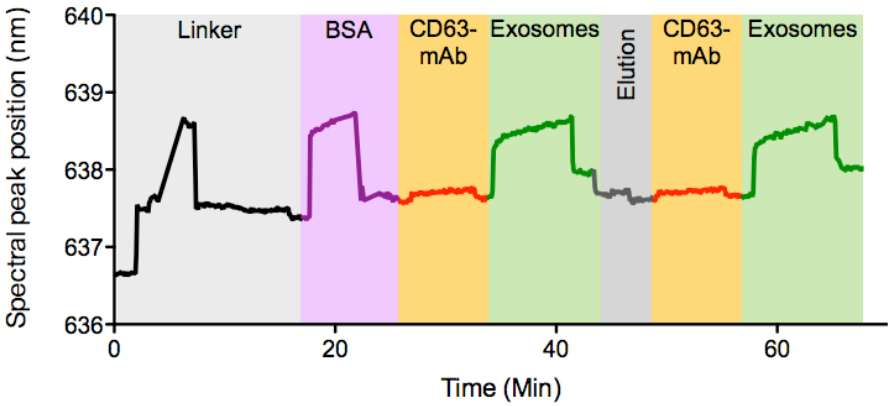

Supplementary Figure 8. Real-time sensorgram. We performed a series of operation, namely surface blocking with bovine serum albumin (BSA), conjugation with CD63 monoclonal antibody (CD63-mAb) and exosome capture, by sequentially flowing reagents to a nPLEX chip. The processes were monitored *in-situ* by tracking the transmission spectral shifts. The entire assay from the antibody-binding to exosome capture was complete in < 30 min. Importantly, the chip surface could be regenerated for repeated uses by eluting antibodies and exosomes.

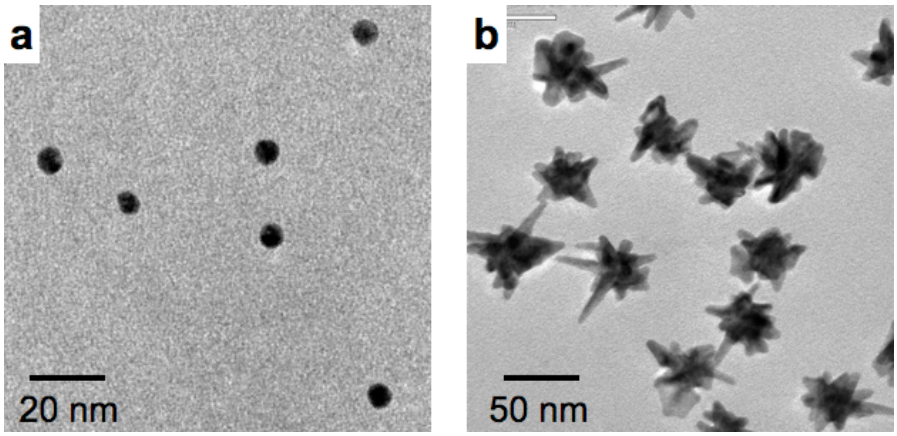

Supplementary Figure 9. Au nanoparticles for signal amplification. Au nanospheres (diameter, 10 nm; a) and star-shaped Au nanoparticles (mean diameter, 50 nm; b) were used as a secondary labeling agent for signal amplification.

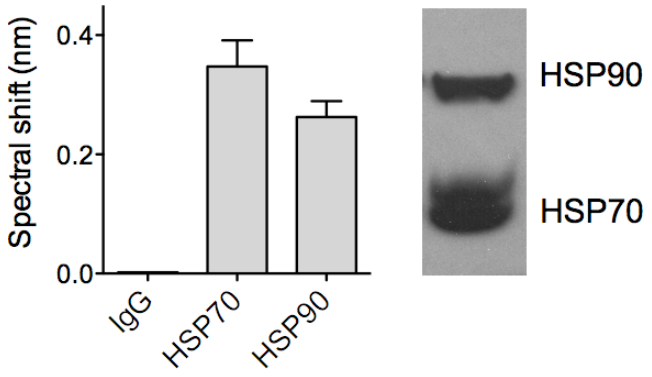

Supplementary Figure 10. nPLEX assay of intravesicular protein markers. For the detection of intravesicular markers, exosomes were lysed, and the lysates were introduced onto the nPLEX chip. The chip had sensing arrays that were separately conjugated with isotype-matched IgG, heat-shock protein (HSP) 70 or HSP90 antibodies. The results from the nPLEX analyses (left) qualitatively matched with western blotting data (right), showing the relative high abundance of HSP70 over HSP90.

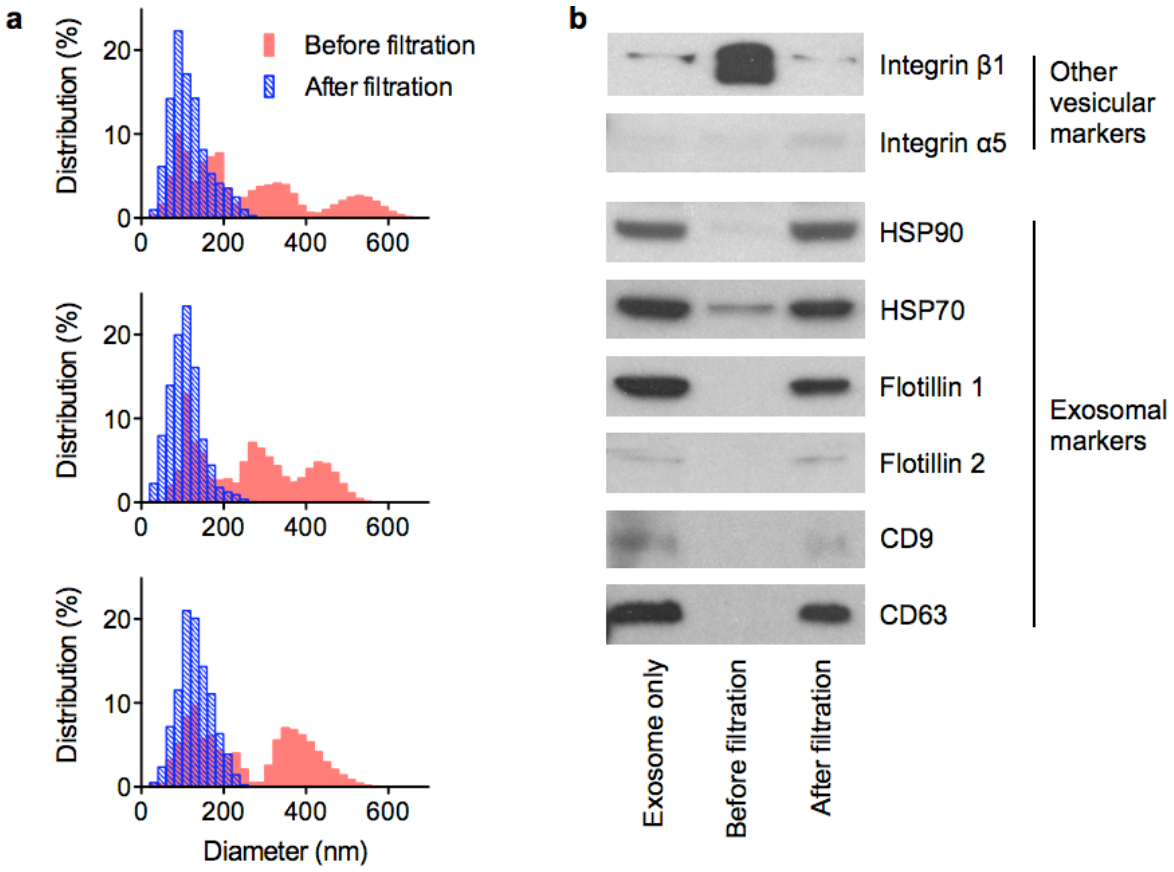

Supplementary Figure 11. **Preparation of exosomes from filtration. (a)** Size distribution of clinical ascites samples, before (pink) and after (blue) filtration steps. A membrane filter with 0.2 μm size cutoff was used to remove large cellular and vesicular debris. Post filtration, a single size peak at ~ 100 nm vesicular diameter was observed for all samples. **(b)** The vesicular composition of membrane filtrate was analyzed. Aliquots of CaOV3 cell culture supernatant were processed via 1) conventional gradient ultracentrifugation to enrich for pure exosomes (Exosome only); 2) direct centrifugal concentration without filtration (Before filtration) and 3) centrifugal concentration after 0.2 μm filtration to remove large debris (After filtration). Lysates from three samples were quantified,and equal protein amounts were immunoblotted for exosomal markers (HSP90, HSP70, Flotillin 1, Flotillin 2, CD9 and CD63) as well as other vesicular markers (Integrin β1, Integrin α5). The results showed that filtration can effectively remove other large vesicular debris while retaining exosomal population for the nPLEX assay, as compared to the positive control (Exosome only).

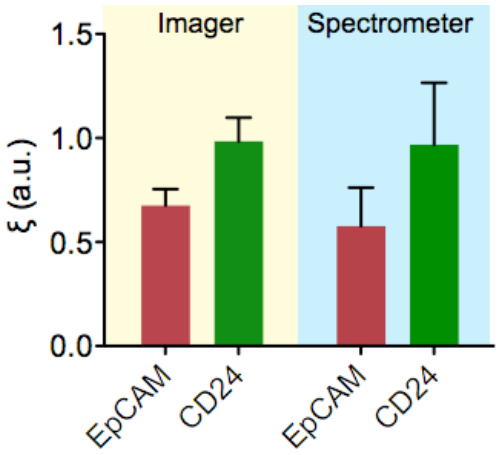

Supplementary Figure 12. **Comparison between intensity and spectrum measurements.** Exosomal protein levels of EpCAM and CD24 measured by the portable nPLEX imager system were compared with those measured by the spectrometer setup with a microscope. The results showed an excellent agreement. a.u., arbitrary unit.

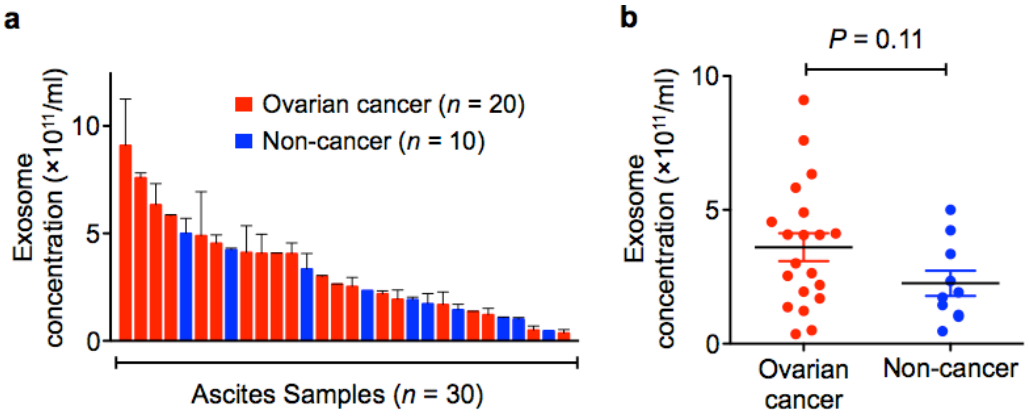

Supplementary Figure 13. Heterogeneity of total exosome concentration in human ascites samples. **(a)** Exosome concentration (from cancer and host cells) was determined in native clinical ascites ($n = 30$) with the nPLEX platform, based on their CD63 spectral shifts ($\Delta\lambda^{CD63}$), and sorted from high to low. Both ovarian cancer ascites and non-cancer ascites samples show a high degree of heterogeneity in exosome concentration with a significant overlap in total numbers. The data is displayed as mean ± s.e.m from triplicate measurements. **(b)** Exosome concentration alone is not sufficient for cancer diagnosis. The mean values from cancer and non-cancer groups were statistically identical ($P = 0.11$, two-tailed unpaired *t*-test).

a

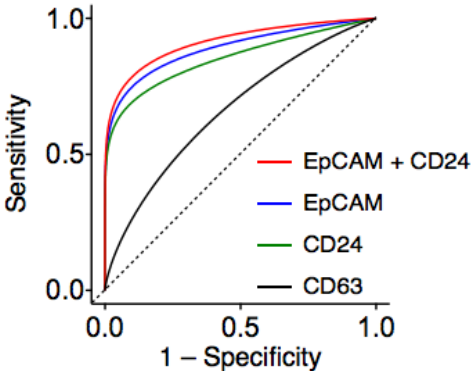

b

Category	Marker	Cutoff value	Sensitivity	Selectivity	Accuracy	AUC
Exosome counts	CD63	0.39	0.75	0.6	0.70	0.670
Protein expression per exosome	EpCAM	0.10	0.90	1.0	0.93	0.968
	CD24	0.09	0.80	1.0	0.87	0.900
	EpCAM + CD24	0.12	0.95	1.0	0.97	0.995

Supplementary Figure 14. Statistical analyses of patient profiling data. (a) Receiver operation characteristic (ROC) curves were generated based on patient profiling data in Fig. 5c (main text). Combining EpCAM and CD24 expression improved overall diagnostic accuracy. **(b)** Diagnostic metrics were determined from ROC curves. The dual marker set (EpCAM and CD24) has the highest detection accuracy of 97%. Note that CD63 alone is a poor diagnostic marker with area under curve (AUC) < 0.7.

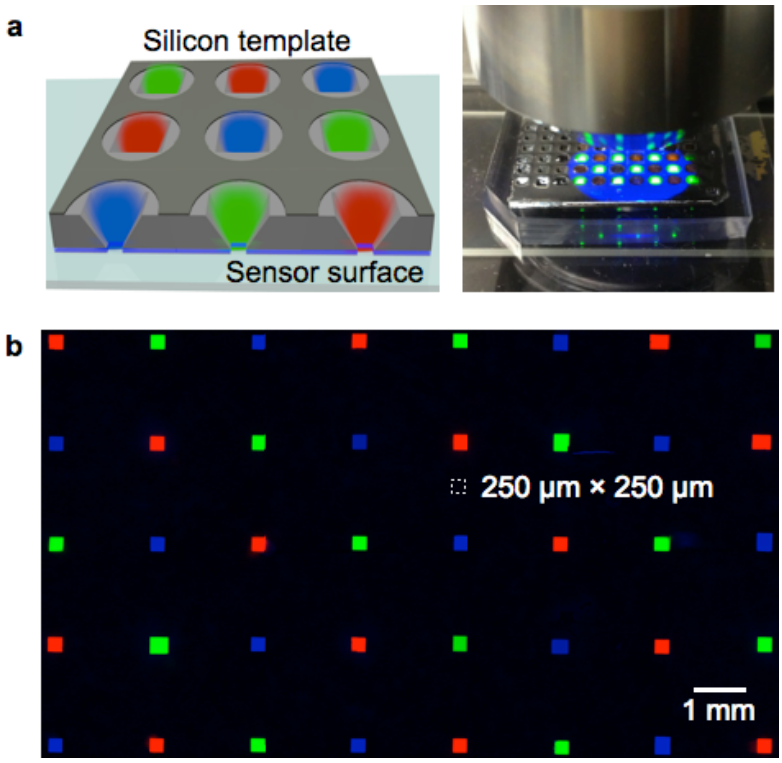

Supplementary Figure 15. Reusable template for molecular printing on nPLEX sensor. (a) A molecular printing template was fabricated by anisotropically etching a (100) Si wafer (Left). While one side of the template had wide window (~ 1 mm × 1 mm) for applying solutions by pipetting or spot-printing, the other side had much confined openings (250 μm × 250 μm) for local delivery of agents to the sensor surface (right). **(b)** As a proof-of-concept, we printed three different types of fluorescent antibodies on a glass substrate, using the developed template. Each spot size is 250 μm × 250 μm.

Supplementary Table 1. List of protein markers and their antibodies used in the profiling.

Protein Marker	Description	Antibody
EpCAM	Epithelial cell adhesion molecule, transmembrane glycoprotein expressed exclusively in epithelial and epithelial derived neoplasms.	Abcam, clone MOC-31
CD24	A small heavily glycosylated cell adhesion molecule, expressed in hematological malignancies and a variety of solid tumors.	eBioscience, clone eBioSN3
CA19-9	Cancer antigen 19-9, a carbohydrate tumor-associated antigen, found in a wide range of malignant conditions including ovarian carcinomas.	Abcam, clone SPM110
CLDN3	Claudin 3, a transmembrane protein crucial in the formation and function of tight junctions, associated with elevated expression in ovarian cancer.	R&D Systems, clone 385021
CA-125	Cancer antigen 125, also known as mucin 16, a member of the mucin family glycoprotein, and is the most frequently used biomarker for ovarian cancer detection.	Abcam, clone X75
MUC18	Mucin 18, a cell surface glycoprotein and cell adhesion molecule whose expression is a prognostic marker in epithelial ovarian cancer.	R&D Systems, clone 128018
EGFR	Epidermal growth factor receptor, a cell-surface receptor whose overexpression and mutations have been associated with many cancers.	Abcam, clone EGFR.1
HER2	Human epidermal growth factor receptor 2, also known as receptor tyrosine kinase erbB-2, whose overexpression plays a major role in the development and progression of multiple cancers.	Biolegend, clone 24D2
CD41	Also known as integrin alpha chain 2b, a heterodimeric integral membrane protein expressed on platelets.	Biolegend, clone HI30
CD45	Encoded by the PTPRC gene, a type I transmembrane protein expressed on all leukocytes.	Biolegend, clone HIP8
D2-40	A surface sialoglycoprotein used to distinguish mesothelial cells from adenocarcinoma.	Abcam, clone D2-40
CD63	A type III lysosomal membrane protein abundant and characteristic in exosomes.	BD Biosciences, clone H5C6

Supplementary Table 2. Clinical information of patients.

Characteristic	Molecular Profile (Fig. 4c) Number (%)	Longitudinal Study (Fig. 4d) Number (%)
Non Cancer Ascites	10	-
Ovarian Cancer	20	8
Age		
Median	60	60
Range	36-85	50-85
Histology		
Serous	16 (80%)	5 (62.5%)
Mucinous	1 (5%)	1 (12.5%)
Mixed	1 (5%)	1 (12.5%)
Poorly Differentiated	2 (10%)	1 (12.5%)
Stage		
IIIC	10 (50%)	5 (62.5%)
IV	10 (50%)	3 (37.5%)
Grade		
1	1 (5%)	0
2	1 (5%)	0
3	18 (90%)	8 (100%)
Surgical Debulking		
Optimal	9 (45%)	4 (50%)
Suboptimal	2 (10%)	1 (12.5%)
Interval	8 (40%)	3 (37.5%)
None	1 (5%)	0
Platinum response		
Sensitive	5 (25%)	2 (25%)
Resistant	14 (70%)	5 (62.5%)
Refractory	1 (5%)	1 (12.5%)
Clinical Trajectory		
Response	3 (15%)	4 (50%)
Stable	1 (5%)	0
Mixed	2 (10%)	0
Progression	14 (70%)	4 (50%)
Existing Therapies		*n* =16*
Carboplatin + Taxol	2 (10%)	2 (12.5%)
Taxol +/- Avastin	5 (25%)	4 (25%)
Carboplatin	1 (5%)	0 (0%)
Doxil	2 (10%)	3 (18.75%)
Topotecan	1 (5%)	0 (0%)
Avastin	0 (0%)	1 (6.25%)
None	9 (45%)	6 (37.5%)
Ascites Volume (*L*)		
(mean / range)	2.8 (1.1 - 6.4)	2.6 (0.4 - 4.5)

*two time points for each patient.

Supplementary Table 3. Clinical information on patient samples used in molecular profiling.

Characteristic	Molecular Profile (Fig. 4c) Number (%)
Non Cancer Ascites	10
Cirrhosis	10 (100%)
Heart failure	0
Ascites Volume (*L*)	
(mean / range)	5.6 (2.0 - 8.8)
Ovarian Cancer	20
Histology	
Serous	16 (80%)
Mucinous	1 (5%)
Mixed	1 (5%)
Poorly Differentiated	2 (10%)
Ascites Volume (*L*)	
(mean / range)	2.8 (1.1 - 6.4)

Supplementary Table 4. Clinical information on patient samples used in treatment monitoring.

Characteristic	Molecular Profile (Fig. 4d) Number (%)
Ovarian Cancer	20
Responders	4 (50%)
Histology	
Serous	2 (50%)
Mucinous	1 (25%)
Mixed	1 (25%)
Poorly Differentiated	0
Stage	
IIIC	1 (25%)
IV	3 (75%)
Ascites Volume (*L*)	
(mean / range)	2.5 (1.0 - 4.5)
Non-Responders	4 (50%)
Histology	
Serous	3 (75%)
Mucinous	0
Mixed	0
Poorly Differentiated	1 (25%)
Stage	
IIIC	3 (75%)
IV	1 (25%)
Ascites Volume (*L*)	
(mean / range)	2.6 (0.4 - 3.9)

Supplementary References

1. Mudanyali, O. et al. Compact, light-weight and cost-effective microscope based on lensless incoherent holography for telemedicine applications. *Lab Chip* **10**, 1417-1428 (2010).
2. Palik, E. D. *Handbook of Optical Constants of Solids: Index* (Access Online via Elsevier, 1998).
3. Sheehan, K. M. et al. Use of reverse phase protein microarrays and reference standard development for molecular network analysis of metastatic ovarian carcinoma. *Mol. Cell. Proteomics* **4**, 346-355 (2005).
4. Skog, J. et al. Glioblastoma microvesicles transport RNA and proteins that promote tumour growth and provide diagnostic biomarkers. *Nat. Cell Biol.* **10**, 1470-1476 (2008).
5. Yuan, H. et al. Gold nanostars: surfactant-free synthesis, 3D modelling, and two-photon photoluminescence imaging. *Nanotechnology* **23**, 075102 (2012).
6. Hill, H. D. & Mirkin, C. A. The bio-barcode assay for the detection of protein and nucleic acid targets using DTT-induced ligand exchange. *Nat. Protoc.* **1**, 324-336 (2006).
7. Campbell, M. T. H. R. G. D. M., Sharp, D. N., Harrison, M. T., Denning, R. G. & Turberfield, A. J. Fabrication of photonic crystals for the visible spectrum by holographic lithography. *Nature* **404**, 53-56 (2000).
8. Henzie, J., Lee, M. H. & Odom, T. W. Multiscale patterning of plasmonic metamaterials. *Nature Nanotech.* **2**, 549-554 (2007).